Article ID: 1003－6326(2004)02－0362－04

Analysis of FCC sheet metal forming with rate-independent polycrystalline plasticity FEM①

ZHANG Shao-rui(张少睿), LI Da-yong(李大永), LUO Ying-bing(罗应兵), PENG Ying-hong(彭颖红)
(School of Mechanical Engineering, Shanghai Jiaotong University, Shanghai 200030, China)

Abstract: A rate-independent polycrystalline plasticity constitutive model considering self and latent hardening was developed. Next, a new orientation probability assignment method was proposed and the crystal orientations were assigned to FE integration points, which represent crystals and can rotate individually. Then cup drawing of FCC aluminum sheet was studied using crystalline plasticity finite element analysis. The results show that the validity of proposed model is proved through comparison between numerical results and experimental ones. {001}〈110〉 texture can lead to earing at 45° direction, while {124}〈211〉 texture at 0° and 90° directions. For the rolled aluminum sheet, which contains strong {001}〈110〉 texture, earing is formed at 45° direction after cup drawing. For the annealing aluminum sheet, due to the balance between two main textures, the flange earing tendency is not obvious.

Key words: FCC sheet metal; rate-independent; texture; polycrystalline plasticity FEM; orientation probability assignment

CLC number: TG 302; TG 111.7 **Document code:** A

1 INTRODUCTION

The anisotropy of sheet metal exerts an evident influence on the formability. It is well known that the plastic anisotropy of sheet metal is usually caused by crystallographic texture, which is developed during mechanical deformation and heat treatment. Therefore the texture should be taken into consideration in the sheet metal simulation for a higher accuracy.

In recent years, great progress has been made in the technology of the crystalline plasticity finite element analysis of sheet metal forming, in which the texture is introduced through the measured crystal morphological data. Anand et al[1] simulated earing in cup drawing of single crystal FCC material. Nakamachi et al[2-7] developed an elastic/polycrystalline viscoplastic finite element program and applied it to the formability analysis of sheet metal. In the above researches, the authors applied a rate-dependent crystal model, without dividing slip systems into active and inactive sets. In fact, the slip systems are activated according to the resolved shear stress on each of them.

In this study, a rate-independent polycrystalline plasticity model is developed and introduced into dynamic explicit element method. A "successive integration method" used to determine slip system is applied to calculation of the plastic strain in this model. Self and latent hardening is taken into account, and an orientation assignment method is proposed. Then cup drawing of aluminum sheet is simulated with the developed rate-independent polycrystalline plasticity FEM program. Flanging earing tendencies with different initial orientations are discussed.

2 RATE-INDEPENDENT CRYSTALLINE PLASTICITY FEM

2.1 Crystalline plasticity constitutive equation

For a slip system s, the initial normal vector of the slip plane is defined by $\boldsymbol{m}^{(s)}$, and the unit slip direction vector by $\boldsymbol{n}^{(s)}$. During the plastic deformation, the crystalline lattice rotates. Then these vectors become $\boldsymbol{m}^{*(s)}$ and $\boldsymbol{n}^{*(s)}$.

The plastic deformation ratio of tensor $\boldsymbol{D}^{\mathrm{p}}$ and rotation tensor ω^{p} are

$$\boldsymbol{D}_{ij}^{\mathrm{p}} = \sum_{s=1}^{M} \boldsymbol{L}_{ij}^{(s)} \dot{\gamma}^{(s)}, \quad \omega_{ij}^{\mathrm{p}} = \sum_{s=1}^{M} \boldsymbol{W}_{ij}^{(s)} \dot{\gamma}^{(s)} \tag{1}$$

where $\dot{\gamma}^{(s)}$ is the strain rate on the slip system s, M is the total number of slip systems, and

$$\boldsymbol{L}_{ij}^{(s)} = \frac{1}{2}(\boldsymbol{m}_i^{*(s)}\boldsymbol{n}_j^{*(s)} + \boldsymbol{n}_j^{*(s)}\boldsymbol{m}_i^{(s)}) \tag{2}$$

$$\boldsymbol{W}_{ij}^{(s)} = \frac{1}{2}(\boldsymbol{m}_i^{*(s)}\boldsymbol{n}_j^{*(s)} - \boldsymbol{n}_j^{*(s)}\boldsymbol{m}_i^{(s)}) \tag{3}$$

The strain rate of deformation tensor $\boldsymbol{D}_{ij}$ can be decomposed as

$$\boldsymbol{D}_{ij} = \boldsymbol{D}_{ij}^{\mathrm{e}} + \boldsymbol{D}_{ij}^{\mathrm{p}} \tag{4}$$

① **Foundation item:** Project(01QMH1411) supported by Shanghai Post-phosphor Foundation; project(2001) supported by Shanghai Post-doctoral Foundation

Received date: 2003－05－22; **Accepted date:** 2003－09－20

Correspondence: ZHANG Shao-rui, PhD candidate; Tel: +86-21-62835728; E-mail: lszsr@8163.net

Then the crystalline plasticity constitutive equation can be expressed as

$$\overset{\nabla}{\sigma}_{ij} = \boldsymbol{C}^{e}_{ijkl}\left(\boldsymbol{D}_{kl} - \sum_{s=1}^{M} \boldsymbol{L}^{(s)}_{kl}\dot{\gamma}^{(s)}\right) \tag{5}$$

where $\overset{\nabla}{\sigma}_{ij}$ is the Jaumman rate of Kirchhoff stress tensor, $\boldsymbol{C}^{e}_{ijkl}$ is the elastic constitutive tensor.

2.2 Calculation of plastic deformation

The resolved shear stress in the slip system s can be calculated with

$$\tau^{(s)} = \boldsymbol{L}^{(s)}_{ij}\sigma_{ij} \tag{6}$$

The Schmid law is given by

$$\mathrm{sgn}(\tau^{(s)})\,\tau^{(s)} = k_s \tag{7}$$

where k_s is the critical yielding stress on the slip system s.

The active slip system can be judged through the following conditions:

$\mathrm{sgn}(\tau^{(s)})\,\dot{\gamma}^{(s)} \geqslant 0$ for active slip systems

$\mathrm{sgn}(\tau^{(s)})\,\tau^{(s)} < k_s$ for inactive slip systems

The key problem of the rate-independent formulation of crystal plasticity is the possible occurrence of redundant constrains due to active slip systems. In order to solve this problem, a "successive integration method"[8] is introduced. For all slip systems, the following differential equations are introduced:

$$2G\cdot(\mathrm{d}X_s/\mathrm{d}\rho) = Y_s \tag{8}$$

where ρ ($\geqslant 0$) is a monotonously increasing parameter such as time, G is shear modulus, and

$$X_s = \mathrm{sgn}(\tau^{(s)})\,\dot{\gamma}^{(s)} \tag{9}$$

$$Y_s = \mathrm{sgn}(\tau^{(s)})\,\boldsymbol{L}^{(s)}_{ij}\sigma_{ij} - k_s \tag{10}$$

The above equations are successively integrated under the following conditions.

1) Initial condition: $X_s = 0$ at $\rho = 0$

2) Constraint condition: when the value of X_s becomes negative during the integration, set $X_s = 0$.

Continue the above integration until X_s remains unchanged. Then each slip system belongs to one of the following two groups:

1) $X_s > 0$ and $\mathrm{d}X_s/\mathrm{d}\rho = 0$ for active systems;

2) $X_s = 0$ and $\mathrm{d}X_s/\mathrm{d}\rho < 0$ for inactive systems.

The algorithm for the numerical computation is as follows:

1) set $\dot{\gamma}^{(s)} = 0$ and $\boldsymbol{D}^{p}_{ij} = 0$;

2) calculate trial stress with Eqn. (5);

3) calculate the trial resolve shear stress in each slip system with Eqn. (6);

4) determine the potentially active systems that satisfy $Y_s \geqslant 0$;

5) obtain $\mathrm{d}X_s$ from Eqn. (8) and we have

$$\dot{\gamma}_{\rho+\mathrm{d}\rho} = \dot{\gamma}_{\rho} + \mathrm{d}\dot{\gamma} \tag{11}$$

6) amend $\boldsymbol{D}^{p}_{ij}$ by Eqn. (2) and update k_s by hardening law;

7) if the convergence of $\boldsymbol{D}^{p}_{ij}$ is not attained, return to step 2).

2.3 Hardening law

During plastic deformation, more than one slip system are activated at the same time, and the slip in each slip system has an effect on the hardening of all systems. The hardening evolution equation in slip system s is expressed as

$$\dot{\tau}_s = \sum_{t} \boldsymbol{h}_{s,t}\,|\dot{\gamma}_t| \tag{12}$$

$$\boldsymbol{h}_{s,t} = \boldsymbol{h}(\gamma)\,\boldsymbol{q}_{s,t} \tag{13}$$

where $\boldsymbol{h}_{s,t}$ is the hardening coefficient, γ is the accumulated shear strain of all the slip systems, $\boldsymbol{q}_{s,t}$ is the interaction matrix describing the self and latent hardening.

Pierce et al[9] expressed $\boldsymbol{q}_{s,t}$ with a simple form as

$$\boldsymbol{q}_{s,t} = q + (1-q)\,\delta_{s,t} \tag{14}$$

where q is the ratio of latent hardening to self hardening, which is assumed as

$$q = \begin{cases} 1, & \text{Coplanar} \\ 1-1.4 & \text{Non-coplanar} \end{cases}$$

2.4 Orientation probability assignment method

In this study, crystals are represented by FE integration points. The orientations determined from the measured ODF (orientation distribution function) data and expressed in term of Euler angles, should be assigned to FE integration points.

The orientation distribution function $f(g)$ can be divided into two parts: normal distribution and random distribution, then it can be written as[10]

$$f(g) = f_{\mathrm{r}}(g) + \sum_{j=1} f_j(g) \tag{15}$$

where $f_{\mathrm{r}}(g)$ is the random distribution function, and $f_j(g)$ is normal distribution function, representing the main texture component with a peak density.

For a main texture component g_i, the volume fraction φ_i of a spreading space around this peak position can be obtained:

$$\varphi_i = \frac{1}{2\sqrt{\pi}} Z_i S_i \psi_i \left[1 - \exp(-\psi_i^2/4)\right] \tag{16}$$

where Z_i is the multiplicity factor, S_i is the peak ODF value of this texture component, and ψ_i is the disperse width.

Here, the fraction of the crystal numbers $N_{\mathrm{f}}^{(i)}$ is assumed to be equal to that of volume in each spreading space:

$$N_{\mathrm{f}}^{(i)} = \frac{N^{(i)}}{N} = \varphi_i \tag{17}$$

where $N^{(i)}$ is the crystal numbers in the ith spreading space and N is the total number of crystallites in the sample. Then the ODF data can be randomly assigned to the FEM integration points one by one.

3 FE ANALYSIS OF CUP DEEP DRAWING

Above rate-independent polycrystalline plasticity

model is introduced into dynamic explicit FEM procedure[11], and a cup drawing problem is adopted to investigate the texture effect on the earing.

The schematic view of the cup drawing process is shown in Fig. 1. The rolled and annealing pure aluminum sheets are selected to study the relation between the preferred orientation and earing.

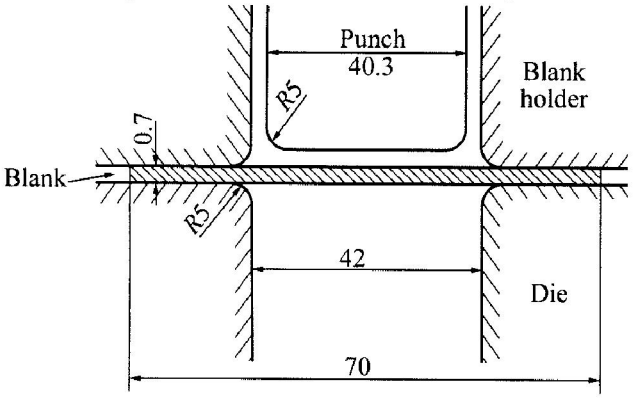

Fig. 1 Geometry and dimension of cup drawing

Pole figures are measured with an automated X-ray texture goniometer at half thickness of the sheets. ODF data expressed with Euler angles $g(\phi_1, \Phi, \phi_2)$ are computed from three incomplete pole figures ({111}, {200} and {220})[12]. The experimental ODF data for rolled and annealing aluminum sheets are illustrated in Fig. 2. As shown in Fig. 2, the rolled sheet contains mainly strong {001}〈110〉 texture, while the annealing one consists of both relatively {001}〈110〉 and {124}〈211〉 texture components.

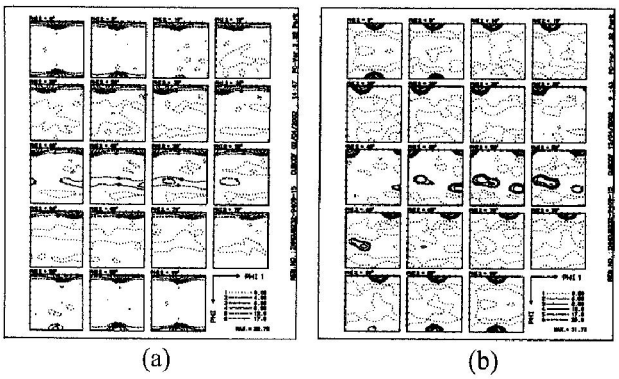

Fig. 2 ODF data of initial rolled and annealing sheet
(a) —Rolled sheet; (b) —Annealing sheet

Based on the above theory, initial orientations are assigned to FE integrations and the cup drawing process of these two sheets is simulated. Other material properties for FCC aluminum are assumed as: elastic modulus E = 69 GPa, Poisson ratio υ= 0.3, sheet thickness t = 0.7 mm. Only a quarter of circular sheet is needed in the calculation because of symmetry, and the sheet is divided into 770 four-node Mindlin shell elements.

The calculated flange configurations after forming are shown in Fig. 3. The cold rolled aluminum sheet shows a strong earing tendency, while the annealing one has no obvious earing tendency.

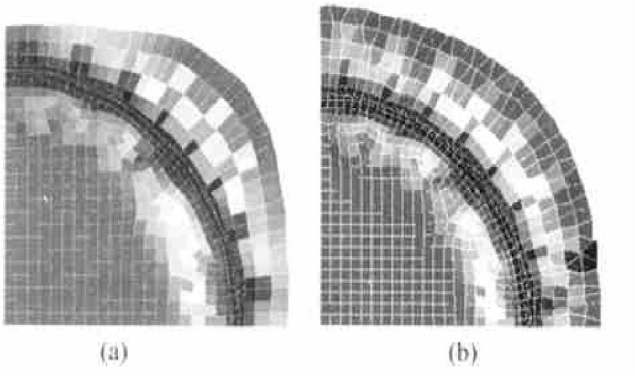

Fig. 3 Earing configurations after deep drawing corresponding to different materials
(a) —Rolled sheet; (b) —Annealing sheet

The ODF figures after drawing can be drawn according to the calculated orientations at integration points which represent crystals. Comparisons of calculated ODF results of these two sheets after forming with experimental ones are shown in Fig. 4 and Fig. 5, respectively. Good consistency can be found. The numerical results have a little stronger congregation and higher ODF peak values. After deep drawing, the {001}〈110〉 texture decreases, and the {124}〈211〉 texture increases.

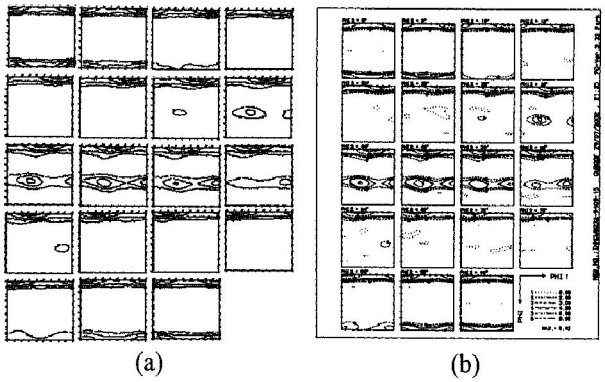

Fig. 4 ODF contour lines of rolled aluminum cup
(a) —Numerical; (b) —Experimental

To investigate further the effect of texture on the earing, two ideal sheets, one containing 100% {001}〈110〉 texture and the other 100% {124}〈211〉 texture, are considered and the forming process of them is simulated. Deformed configurations are shown in Fig. 6. It can be seen that single {001}〈110〉 texture can result in earing in 45° direction and single {124}〈211〉 texture can result in earing in 0° and 90° directions.

Since the {001}〈110〉 texture in rolled aluminum sheet is much stronger than {124}〈211〉 texture and takes more volume fraction, which leads to a strong anisotropy(earing) formed in 45° direction after drawing. The annealing sheet contains stronger

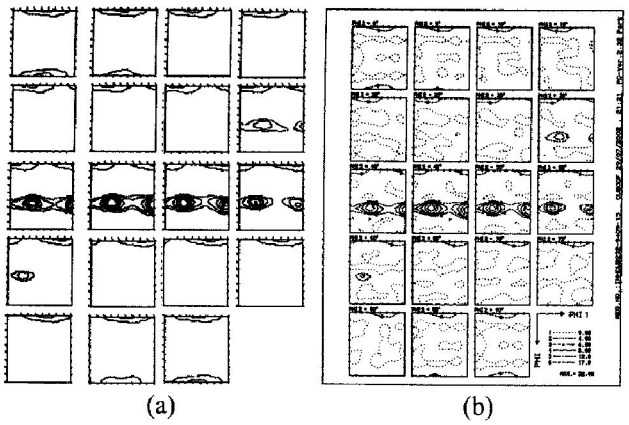

Fig. 5 ODF contour lines of annealing sheet after forming
(a) —Numerical; (b) —Experimental

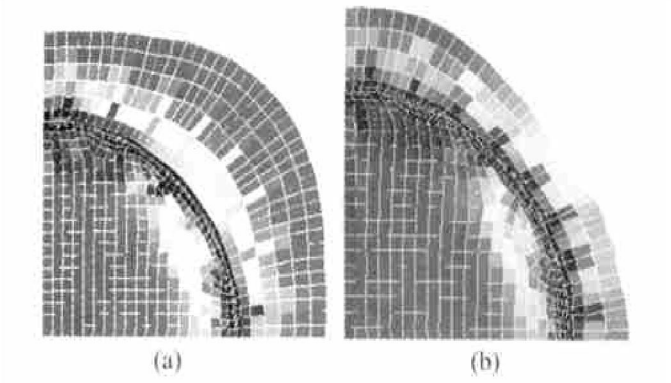

Fig. 6 Earing configurations after deep drawing corresponding to different textures
(a) —{001}〈110〉 texture; (b) —{124}〈211〉 texture

{124}〈211〉 texture than {001}〈110〉 texture, but for the {001}〈110〉 texture takes more volume fraction, so a balance between the effect of these two textures can be obtained and no obvious earing is found.

4 CONCLUSIONS

1) A rate-independent polycrystalline plasticity constitutive model is developed and introduced into dynamic explicit finite element code. An orientation probability assignment method is implemented for the direct use of measured ODF data to the crystalline FE modeling. The FE analyses show a good consistency with the experimental observations, through which the capacity of proposed polycrystalline plasticity model to predict sheet metal formability is confirmed.

2) Numerical analyses reveal that the {001}〈110〉 texture can result in earing at 45° direction, while the {124}〈211〉 texture at 0° and 90° direction. For the rolled aluminum sheet, which contains strong {001}〈110〉 texture, earing is formed at 45° direction after cup drawing. For the annealing aluminum sheet, due to the balance between two main textures, the flange earing tendency is not obvious.

REFERENCES

[1] Anand L, Balasubramanian S. Polycrystal plasticity: application to earing in cup drawing[J]. Annals of the CIRP, 1996, 45(1): 263-268.

[2] Xie C L, Nakamachi E. Investigations of the formability of BCC steel sheets by using crystalline plasticity finite element analysis[J]. Materials and Design, 2002, 23: 59-68.

[3] Nakamachi E, Xie C L, Harimato M. Drawability assessment of BCC steel by using elastic/crystalline viscoplastic finite element analysis[J]. Int J Mech Sci, 2001, 43: 631-652.

[4] Nakamachi E, Hiraiwa K, Morimoto H, et al. Elastic/crystalline viscoplastic finite element analyses of single- and poly-crystal sheet deformations and their experimental verification[J]. Int J Plast, 2000, 16: 1419-1441.

[5] Nakamachi E, Dong X. Elastic/crystalline viscoplastic finite element analysis of dynamic deformation of sheet metal[J]. Int J Computer-Aided Engrg Software, 1996, 13: 308-326.

[6] Nakamachi E, Dong X. Study of texture effect on sheet failure in a limit dome height test by using elastic/crystalline viscoplastic finite element analysis[J]. J Appl Mech Trans ASME(E), 1997, 64: 519-524.

[7] Nakamachi E, Huo T. Dynamic-explicit elastic plastic finite-element simulation of hemispherical punch-drawing of sheet metal[J]. Engineering Computations, 1996, 13: 327-338.

[8] Takahashi H. Stress—strain relations of polycrystalline metals: 3 proportional loading of FCC metals[J]. Bull J Soc Mech Eng, 1976, 19: 1115-1132.

[9] Pierce D, Asaro R J, Needleman A. Material rate dependent and localized deformation in crystalline solids[J]. Acta Metall, 1983, 31: 1951-1972.

[10] Lueke K, Pospiech J, Virnich K H, et al. On the problem of the reproduction of the true orientation distribution from pole figures[J]. Acta Metall, 1981, 29: 167-185.

[11] LI Da-yong, HU Ping, WANG Jin-cheng. An effective numerical method for drawhead force of stamping sheet metals[J]. Chinese Journal of Applied Mechanics, 2001, 18(1): 58-64.

[12] Bunge H J. Texture Analysis in Material Science[M]. London: Butterworths, 1982.

(Edited by YANG Bing)